ACS APPLIED MATERIALS & INTERFACES

Research Article

www.acsami.org

Finding the Lost Open-Circuit Voltage in Polymer Solar Cells by UV-Ozone Treatment of the Nickel Acetate Anode Buffer Layer

Fuzhi Wang,[†] Gang Sun,[†] Cong Li,[†] Jiyan Liu,[‡] Siqian Hu,[‡] Hua Zheng,[§] Zhan'ao Tan,*[,†] and Yongfang Li*[,∥]

[†]State Key Laboratory of Alternate Electrical Power System with Renewable Energy Sources, Beijing Key Laboratory of Energy Security and Clean Utilization, North China Electric Power University, Beijing 102206, China

[∥]Beijing National Laboratory for Molecular Sciences, Institute of Chemistry, Chinese Academy of Sciences, Beijing 100190, China

[‡]Key Laboratory of Optoelectronic Chemical Materials and Devices of Ministry of Education, Jianghan University, Wuhan 430056, China

[§]School of Chemical Engineering, Wuhan University of Technology, Wuhan 430070, China

Supporting Information

ABSTRACT: Efficient polymer solar cells (PSCs) with enhanced open-circuit voltage (V_{oc}) are fabricated by introducing solution-processed and UV-ozone (UVO)-treated nickel acetate (O-NiAc) as an anode buffer layer. According to X-ray photoelectron spectroscopy data, NiAc partially decomposed to NiOOH during the UVO treatment. NiOOH is a dipole species, which leads to an increase in the work function (as confirmed by ultraviolet photoemission spectroscopy), thus benefitting the formation of ohmic contact between the anode and photoactive layer and leading to increased V_{oc}. In addition, the UVO treatment improves the wettability between the substrate and solvent of the active layer, which facilitates the formation of an upper photoactive layer with better morphology. Further, the O-NiAc layer can decrease the series resistance (R_s) and increase the parallel resistance (R_p) of the devices, inducing enhanced V_{oc} in comparison with the as-prepared NiAc-buffered control devices without UVO treatment. For PSCs based on the P3HT:PCBM system, V_{oc} increases from 0.50 to 0.60 V after the NiAc buffer layer undergoes UVO treatment. Similarly, in the P3HT:ICBA system, the V_{oc} value of the device with a UVO-treated NiAc buffer layer increases from 0.78 to 0.88 V, showing an enhanced power conversion efficiency of 6.64%.

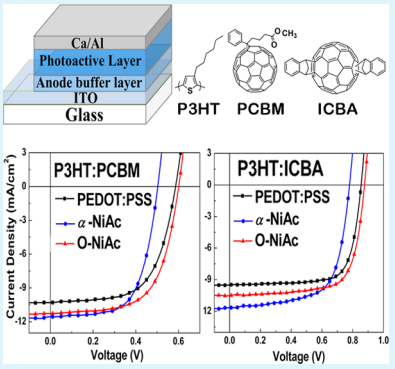

KEYWORDS: *polymer solar cells, anode buffer layer, nickel acetate, UV-ozone treatment*

1. INTRODUCTION

Polymer solar cells (PSCs) have attracted considerable attention because of their potential application in low-cost and large-scale modules.[1−3] In recent years, the power conversion efficiency (PCE) of PSCs has been greatly improved,[4−6] and a PCE of higher than 9% has been reported.[4,6] Recent studies suggest that the interface formed between the active layer and electrode is closely related to the performance and stability of PSCs. Suitable interface materials could adjust the energetic barrier height between the active layer and electrode, which increases the selectivity of the corresponding electrode for carriers (holes or electrons) of one sort. The interface layer can improve the carrier collection efficiency from the two aspects of thermodynamics and kinetics.[7] From the viewpoint of thermodynamics, the ionization potential and electron affinity of the interlayer materials relative to the hole- or electron-transport energies of the active layer could constraint collection of the electrons or holes.[8] From the viewpoint of kinetics, the interlayer material could selectively enhance the collection rate of the electrons or holes over the other.[7] In addition, the interface layer could improve the rectification ratio of the PSCs[9−12] and also plays an important role in balancing the hole and electron harvesting rates at both corresponding electrodes.[13,14] Therefore, when appropriate interfacial materials are chosen, the transportation and collection of either carrier type can be selectively suppressed or enhanced.

Poly(3,4-ethylenedioxythiophene):poly(styrenesulfonate) (PEDOT:PSS) is the commonly used anode modification material. However, the hygroscopic and acidic properties of PEDOT:PSS make it unsuitable for stable PSCs. In recent years, some solution-processed metal oxides, such as MoO_x,[15−19] NiO_x,[20−22] CuO_x,[23] ReO_x,[24] VO_x,[25,26] SnO_x,[27] WO_3,[28] and RuO_x,[29] have been demonstrated as promising alternatives to PEDOT:PSS.

In our previous studies,[30,31] water-soluble nickel acetate [$Ni(CH_3COO)_2$, NiAc] was directly used as an anode buffer layer for PSCs based on the P3HT:PCBM and P3HT:ICBA systems. PSCs with a NiAc anode buffer layer show dramatic enhancement in the short-circuit current density (J_{sc}) while

Received: March 26, 2014
Accepted: May 30, 2014
Published: May 30, 2014

keeping the fill factor (FF) at a relatively high level. Unfortunately, the open-circuit voltage (V_{oc}) of NiAc-modified devices decreased in comparison with PEDOT:PSS-modified devices. V_{oc} of the P3HT:PCBM- and P3HT:ICBA-based devices decreased by 0.09 and 0.07 V,[30,31] respectively. Thus, the overall PCE of the NiAc-based devices is just comparable to that of the PEDOT:PSS-based devices.

As we all know, PCE can be expressed as PCE = $V_{oc}J_{sc}$FF. To further improve the PCE of the NiAc-modified devices, on the basis of greatly enhanced J_{sc} and relatively high FF, optimization of V_{oc} is of the utmost importance. For bulk-heterojunction PSCs in which ohmic contacts are formed with both electrodes, the maximum limit of V_{oc} is governed by the difference between the lowest unoccupied molecular orbital (LUMO) of the acceptor and the highest occupied molecular orbital (HOMO) of the donor, which can be expressed by an empirical equation:[32] $V_{oc} = 1/q(|E_{HOMO,D}| - |E_{LUMO,A}|) - 0.3V$. On the other hand, V_{oc} will be reduced if nonohmic contact is formed at the interface of either or both electrodes of the PSCs, and the value of V_{oc} is equal to the work function (WF) difference of the two electrodes according to the metal−insulator−metal model. Therefore, for PSCs with a given material system, the key to obtaining high V_{oc} is the formation of ohmic contacts at the interface of both electrodes. In addition, some other factors also affect V_{oc}, such as the parallel resistance (R_p)[33] and carrier recombination.[34,35] Both a decrease in R_p and an increase in the carrier recombination lead to reduced V_{oc} and increased dark current under reverse bias.

UV-ozone (UVO) treatment, similar to oxygen-plasma treatment, is a very effective approach to enhancing the WF of electrodes or buffer layers. When indium−tin oxide (ITO) is used as an anode for PSCs, UVO or oxygen-plasma treatment is an essential process to obtain a high WF for efficient hole collection.[36] To achieve better performance for PSCs, UVO treatment is also performed on various electrode buffer layers to achieve a suitable WF. UVO treatment to PEDOT:PSS results in the formation of a metastable surface dipole,[37] which leads to an enhancement in the WF, thus increasing hole extraction from the photoactive layer.[38] The WF of the ZnO electron-transport layer can also be improved after UVO treatment, which enhances charge transport and PCE.[39] In-depth research has been performed on the effect of UVO or oxygen-plasma treatment on solution-processed nickel-containing complexes.[7,40,44] Oxygen-plasma treatment to a NiO_x film, which is obtained from thermal decomposition (250−300 °C) of a solution-deposited nickel precursor, leads to the formation of NiOOH on the surface.[7,44] However, the high-temperature annealing process is not suitable for the fabrication of flexible PSCs with a polymer substrate. Recently, Ma et al. have reported that a solution-processed NiAc precursor can be converted to nickel oxide (Ni_2O_3 and NiO) and NiOOH by the application of thermal annealing (below 150 °C) and UVO simultaneously.[40] It is confirmed that the formation of a favorable NiOOH surface dipole leads to an increase in the WF, resulting in enhanced device performance.

In this work, we processed the as-prepared NiAc film solely by UVO treatment. For the convenience of discussion, the NiAc samples before and after UVO treatment are denoted as α-NiAc and O-NiAc. The X-ray photoelectron spectroscopy (XPS) results confirmed that only a small portion of the NiAc molecules decomposed into NiOOH under UVO treatment, while most of the NiAc precursor remained unchanged. Experimental results show that the small amount of NiOOH on the surface can regulate the energy level alignment at the interface, leading to ohmic contact at the anode interface. At the same time, the UVO treatment further improves the wettability between the substrate and 1,2-dichlorobenzene solvent, which facilitates the formation of an upper photoactive layer with better morphology, inducing a suppressed leakage current. All of these effects induce an enhanced V_{oc} in comparison with the α-NiAc-buffered control devices. For PSCs based on the P3HT:PCBM system, V_{oc} increases from 0.50 to 0.60 V after the NiAc buffer layer undergoes UVO treatment. Similarly, in the P3HT:ICBA system, V_{oc} of the device with a UVO-treated NiAc buffer layer increases from 0.78 to 0.88 V, showing an enhanced PCE of 6.64%.

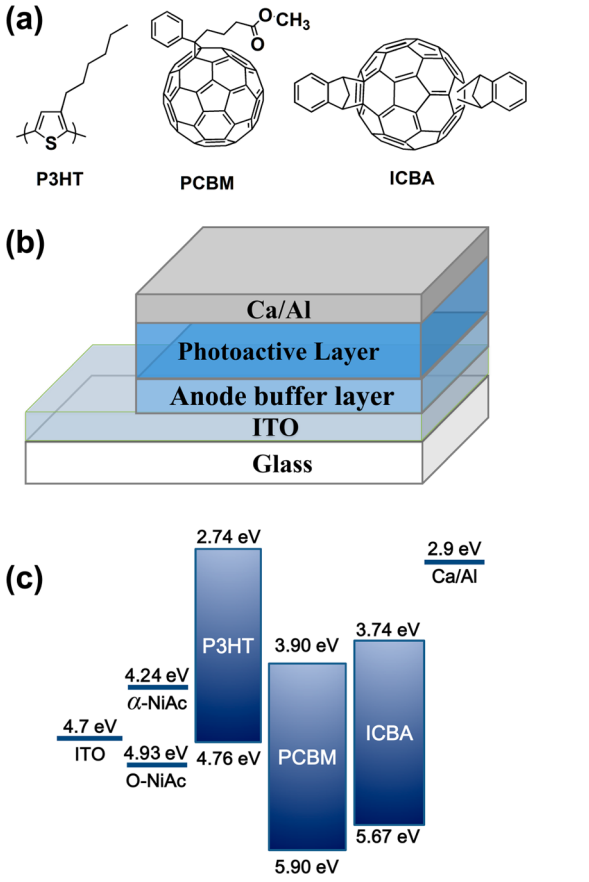

Figure 1. (a) Molecular structures of P3HT, PCBM, and ICBA. (b) Device structure of the PSCs. (c) HOMO and LUMO energy levels of the materials involved in the PSCs.

2. EXPERIMENTAL DETAILS

Six types of devices were designed as follows: (A) ITO/PEDOT:PSS/P3HT:PCBM/Ca/Al, (B) ITO/α-NiAc/P3HT:PCBM/Ca/Al, (C) ITO/O-NiAc/P3HT:PCBM/Ca/Al, (D) ITO/PEDOT:PSS/P3HT:ICBA/Ca/Al, (E) ITO/α-NiAc/P3HT:ICBA/Ca/Al, and (F) ITO/O-NiAc/P3HT:ICBA/Ca/Al. Devices A and D are control devices with PEDOT:PSS as the anode buffer layer, and devices B and E are control devices with α-NiAc as the anode buffer layer. In addition to checking the effect of UVO treatment on the performance of the PEDOT:PSS-based devices, we also fabricated devices with UVO-treated PEDOT:PSS as the anode buffer layer. For device fabrication, a patterned ITO glass substrate (10 Ω $\square^{-1}$) was cleaned by ultrasonic treatment in detergent, deionized water, acetone, and isopropyl alcohol, sequentially. Then, the ITO substrate was treated with UVO for 15 min to remove organic residue. For control devices A and D, a PEDOT:PSS (Clevios P VP AI 4083) aqueous solution was spin-coated

dx.doi.org/10.1021/am5017705 | ACS Appl. Mater. Interfaces 2014, 6, 9458−9465

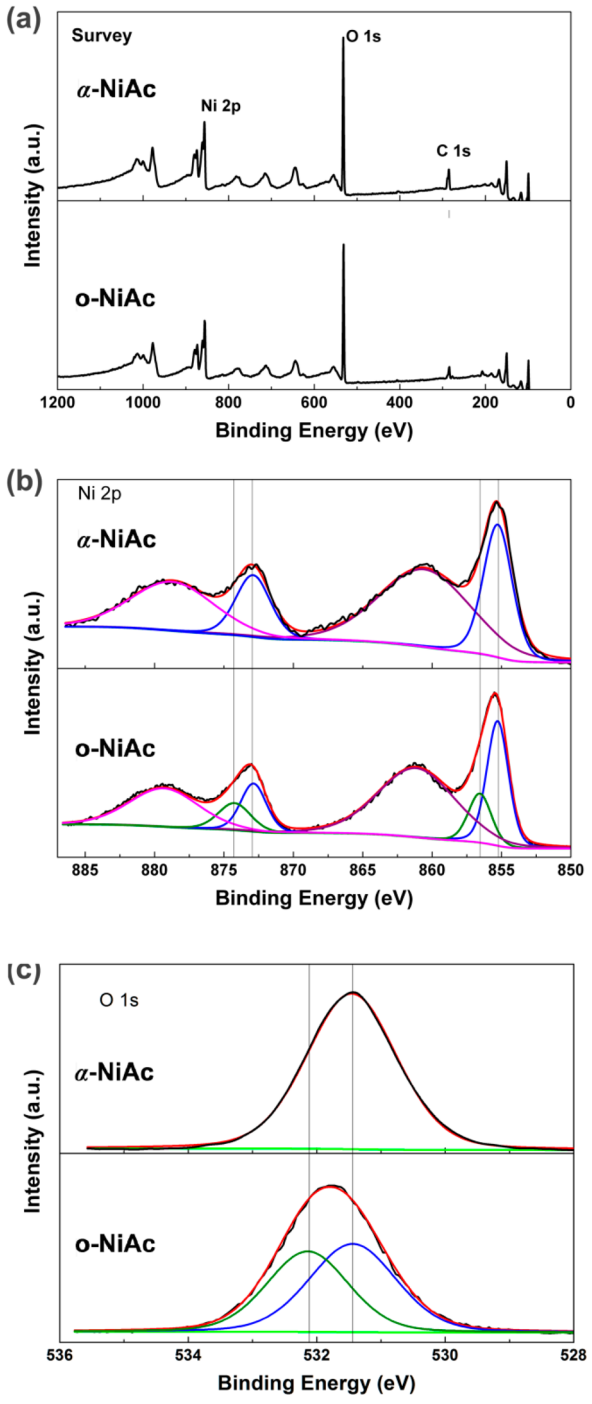

Figure 2. XPS of α-NiAc and O-NiAc: (a) survey scan and (b) Ni 2p and (c) O 1s core-level spectra.

on the pretreated ITO substrate and then annealed at 150 °C for 10 min in air. For devices B and E, the NiAc film was fabricated by spin-coating a nickel acetate tetrahydrate [$Ni(CH_3COO)_2{\cdot}4H_2O$] aqueous solution with a concentration of 1.25 mg mL^{-1} on the pretreated ITO substrate, followed by annealing in air at 150 °C for 10 min to remove the water of crystallization. For devices C and F, the as-prepared NiAc film was further treated with UVO for 15 min. Polymer P3HT and fullerene derivatives (PCBM or ICBA) were used as donor and acceptor materials, respectively. The photoactive layers were fabricated by spin-coating a 1,2-dichlorobenzene solution of P3HT:PCBM or P3HT:ICBA [1:1 (w/w); polymer concentration of 20 mg mL^{-1}] on the modified ITO substrate, followed by solvent annealing in covered glass Petri dishes for 2 h. The thickness of the photoactive layers is around 230 nm. Finally, 10 nm of calcium and a 100 nm of aluminum were deposited through vapor deposition.

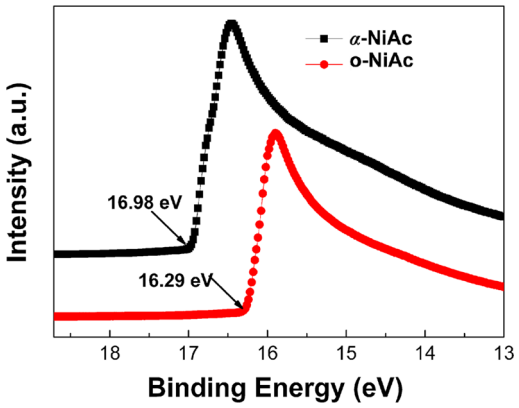

Figure 3. Secondary electron cutoff region of the UPS spectra of the as-prepared and UVO-treated NiAc film on a pretreated ITO substrate.

The current density−voltage (J−V) characteristics of the PSCs were carried out under a nitrogen atmosphere in a glovebox, using a Keithley 236 Source Measure Unit under simulated AM1.5G solar irradiation with a light intensity of 100 mW cm^{-2} (from Newport Co., Ltd.). XPS was performed with an ESCA Lab220i-XL electron spectrometer (base pressure of about 3×10^{-9} mbar) from VG Scientific using 300 W Al Kα radiation to characterize the surface component of the sample. Tapping-mode atomic force microscopy (AFM) was carried out on a Veeco DICP-II instrument. Ultraviolet photoemission spectroscopy (UPS) was performed using an ESCA Lab250xi electron spectrometer under a pressure of about 2×10^{-10} Pa. A He I (21.22 eV) radiation line from a discharge lamp was used in UPS, and the energy resolution was 0.02 eV.

3. RESULTS AND DISCUSSION

The molecular structures of P3HT, PCBM, and ICBA are shown in Figure 1a. The device configuration and energy-level alignment of the materials involved are shown in parts b and c of Figure 1, respectively. The WF of α-NiAc and O-NiAc is determined by UPS. The HOMO and LUMO levels for P3HT,[41] PCBM,[42] and ICBA[43] are from published literature.

XPS measurement was used to investigate the chemical component of the nickel complex film. The samples were all treated at 150 °C for 10 min to remove the water of crystallization before characterization. Figure 2 shows the survey and high-resolution spectra of the Ni 2p, C 1s, and O 1s signals of α-NiAc and O-NiAc. The characteristic peaks of the elements nickel, oxygen, and carbon are shown in the survey scan (Figure 2a). The background was subtracted from the XPS spectra by using a Shirley-type background subtraction. For the sample of α-NiAc, both the Ni $2p_{3/2}$ peak at 855.8 eV and the O 1s peak at 531.4 eV show single and symmetric peaks, indicating that the decomposition of NiAc is negligible during the process of thermal annealing. For the sample O-NiAc, a peak at 856.5 eV appears for the Ni $2p_{3/2}$ peak, which corresponds to the Ni $2p_{3/2}$ orbital of nickel(III) in NiOOH. A pair of peaks with binding energies of 532.1 and 531.4 eV correspond to O 1s in NiOOH and the undecomposed NiAc, respectively.[40] According to changes in the Ni 2p and O 1s core level peaks, it can be concluded that some of NiAc decomposed into NiOOH during the UVO treatment. The result is consistent with the previous literature.[7,40]

UPS measurements were conducted to determine the WF of α-NiAc and O-NiAc (Figure 3). The WF of the nickel complex

dx.doi.org/10.1021/am5017705 | ACS Appl. Mater. Interfaces 2014, 6, 9458−9465

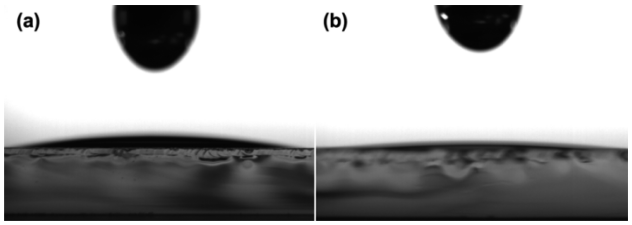

Figure 4. Contact angle of 1,2-dichlorobenzene on (a) α-NiAc and (b) O-NiAc surfaces, respectively.

film can be significantly increased from 4.24 eV for α-NiAc to 4.93 eV for O-NiAc. According to XPS data, NiAc is partially converted into NiOOH, which results in an interface dipole, thus leading to an increase in the WF.[7,40] The increased WF is beneficial to the formation of ohmic contact between the anode and photoactive layer, thus leading to higher V_{oc}.

In order to study the effect of the UVO treatment on the wettability of the NiAc buffer layer toward subsequent deposition of a photoactive layer, the contact angle between the α-NiAc- or O-NiAc-modified ITO substrate and 1,2-dichlorobenzene liquid was measured. As shown in Figure 4b, nearly complete wetting is obtained on the O-NiAc surface with a wetting angle of about 0°, which facilitates the formation of a more uniform active layer.

The morphology of the modified substrate and photoactive layer is characterized by the tapping-mode AFM. As shown in Figure 5, the root-mean-square (rms) roughness of the ITO/α-NiAc (2.65 nm) and ITO/O-NiAc (2.32 nm) substrates is slightly higher than that (1.82 nm) of the PEDOT:PSS-buffered ITO substrate. However, the roughness of the photoactive layer can be dramatically reduced after the nickel complex buffer layer is processed by UVO treatment. Upon UVO treatment to the NiAc film, the rms roughness of the P3HT:PCBM blend film is reduced from 15.7 nm (Figure 5e) to 8.65 nm (Figure 5f), even lower than that of the blend layer on the PEDOT:PSS buffer layer (12.7 nm). Similarly, the rms roughness of the P3HT:ICBA active layer is reduced from 18.9 nm (Figure 5h) to 12.2 nm (Figure 5i). The results indicate that a smoother photoactive film can be realized by UVO treatment of the NiAc buffer, which enables a more uniform interfacial contact between the photoactive layer and cathode, thus increasing the charge collection efficiency.

The PSCs with different buffer layers exhibit different $J-V$ characteristics. Figure 6 shows the $J-V$ curves of the PSCs under illumination of AM1.5G, 100 mW cm^{-2}, and in the dark.

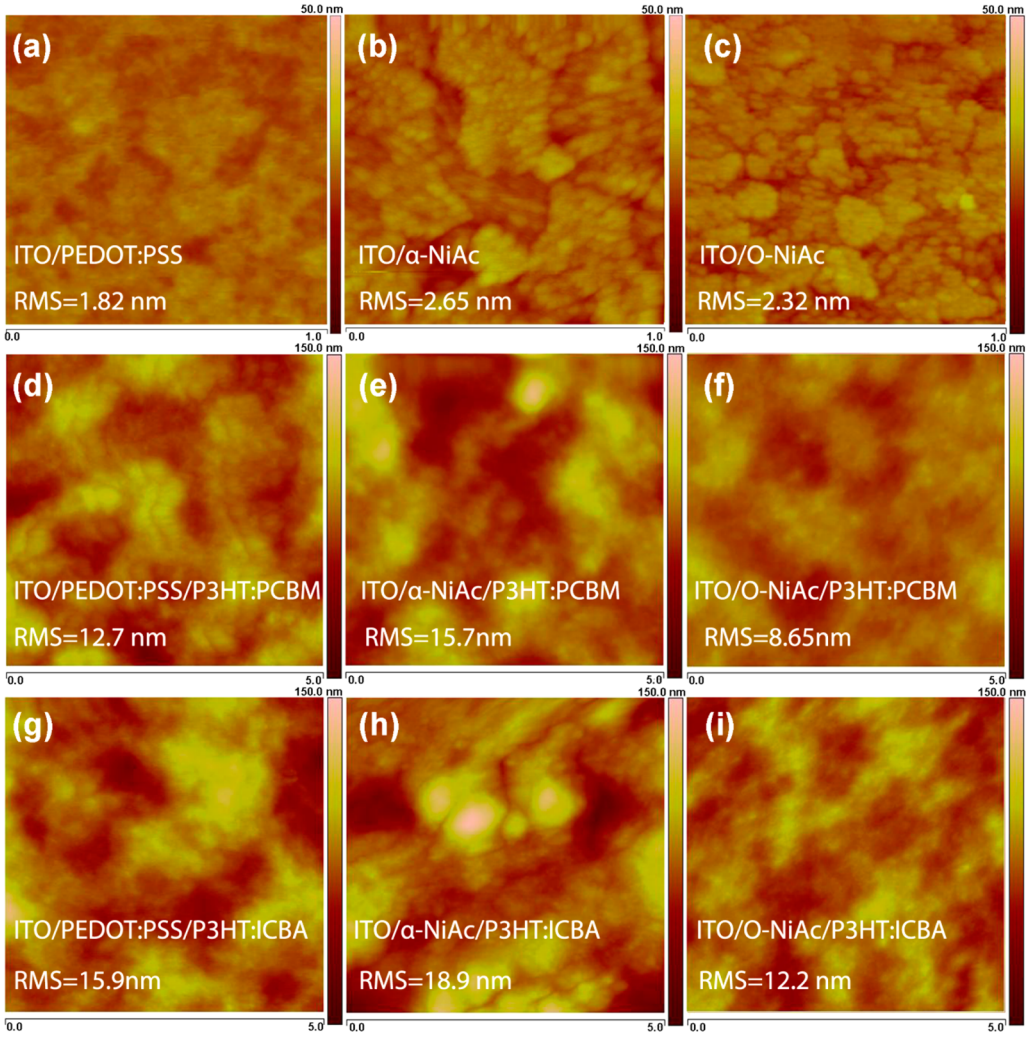

Figure 5. AFM images of (a) PEDOT:PSS, (b) α-NiAc, and (c) O-NiAc on the ITO substrate, P3HT:PCBM on (d) ITO/PEDOT:PSS, (e) ITO/α-NiAc, and (f) ITO/O-NiAc substrates, and P3HT:ICBA on (g) ITO/PEDOT:PSS, (h) ITO/α-NiAc, and (i) ITO/O-NiAc substrates.

dx.doi.org/10.1021/am5017705 | ACS Appl. Mater. Interfaces 2014, 6, 9458−9465

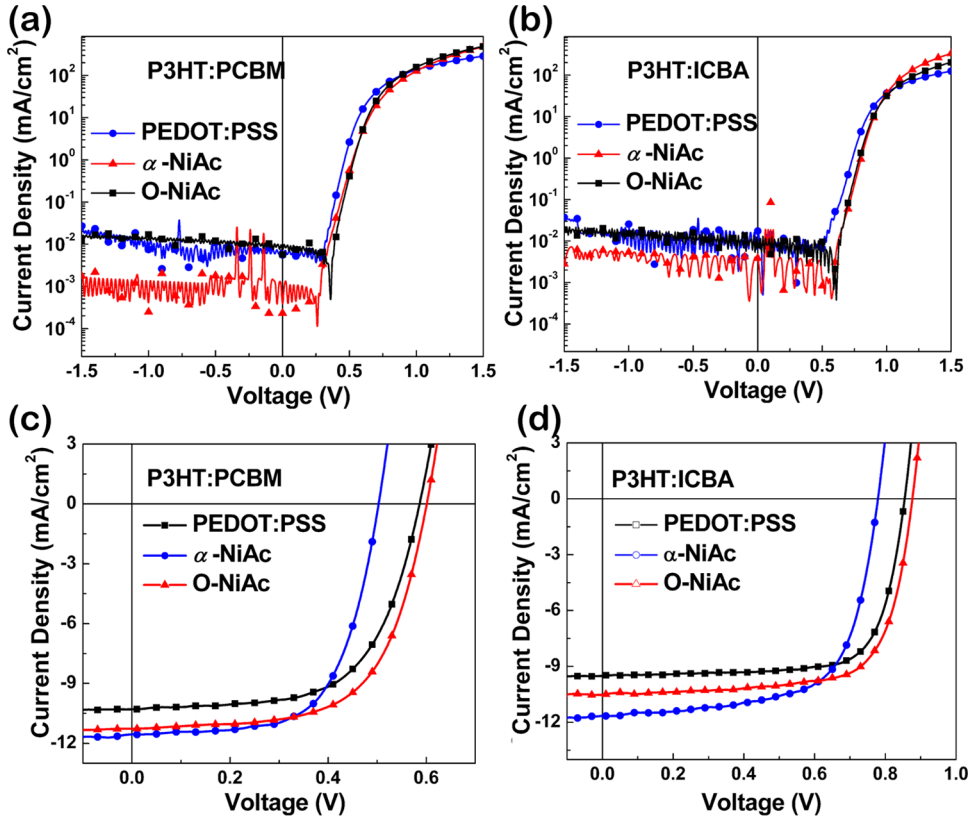

Figure 6. $J-V$ curves of the PSCs based on P3HT:PCBM and P3HT:ICBA: (a and b) under dark conditions; (c and d) under illumination of AM1.5G, 100 mW cm^{-2}.

Table 1. Device Parameters of the PSCs with Different Buffer Layers in the Dark and under Illumination of AM1.5G, 100 mW cm^{-2}

					PCE (%)			
photoactive layer	buffer layer	V_{oc} (V)	J_{sc} (mA cm^{-2})	FF (%)	best	average[a]	R_s[b] (Ω cm^2)	R_p[b] (kΩ cm^2)
P3HT:PCBM	A: PEDOT:PSS[c]	0.59	10.19	63	3.77	3.62 ± 0.03	4.2	93.6
	B: α-NiAc[c]	0.50	11.36	66	3.76	3.66 ± 0.03	3.1	177.8
	C: O-NiAc	0.6	11.22	61	4.13	3.97 ± 0.03	2.0	437.6
P3HT:ICBA	D: PEDOT:PSS[c]	0.85	9.52	75	6.06	5.92 ± 0.04	3.6	42.8
	E: α-NiAc[c]	0.78	11.74	66	6.08	5.92 ± 0.05	4.7	41.5
	F: O-NiAc	0.88	10.55	72	6.64	6.52 ± 0.03	2.8	410.2

[a]The parameters of the PCEs were averaged over 10 PSCs. [b]The parallel resistance (R_p) and series resistance (R_s) for PSCs in the dark are obtained at around 0 and 1 V, respectively. [c]Device parameters of the control devices are cited from our previously published articles.[22,23]

The device parameters are listed in Table 1. In order to investigate the effect of the O-NiAc buffer layer, the $J-V$ behaviors of the devices in the dark (Figure 6a,b) are compared. The slopes of the $J-V$ curves under dark conditions at 0 and 1 V are used to estimate the series resistance (R_s) and shunt resistance (R_p), respectively. The PEDOT:PSS- and α-NiAc-modified devices show the leakage current with the same order of magnitude, which suggests that α-NiAc exhibits buffer and modification functions similar to those of PEDOT:PSS. The leakage current can be decreased by an order of magnitude upon using O-NiAc as the anode buffer layer, which leads to a greatly increased R_p of approximately 537.6 kΩ cm^2. This R_p value is large enough to reduce the power loss by suppressing the leakage current under reversed bias and is critical to the realization of high V_{oc}. R_s consists of the bulk resistance originating from the photoactive layer, buffer layer, and electrodes, and the contact resistance originates from the interface between the electrodes and photoactive layer, which influences the device performance. R_s values of the O-NiAc-buffered PSCs

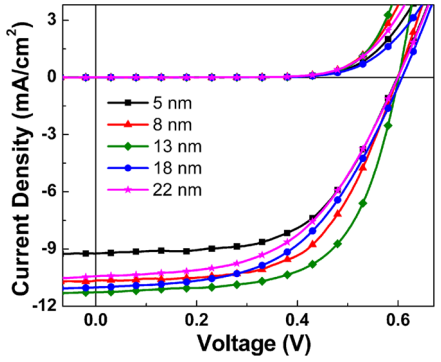

Figure 7. $J-V$ curves of the P3HT:PCBM-based PSCs with different O-NiAc thicknesses in the dark and under illumination of AM1.5G, 100 mW cm^{-2}.

dx.doi.org/10.1021/am5017705 | ACS Appl. Mater. Interfaces 2014, 6, 9458−9465

Table 2. Device Parameters of P3HT:PCBM-Based PSCs with Different O-NiAc Thicknesses

NiAc thickness (nm)	V_{oc} (V)	J_{sc} (mA cm^{-2})	FF (%)	PCE (%) best	PCE (%) average[a]	R_s[b] (Ω cm^2)	R_p[b] (kΩ cm^2)
5	0.6	9.26	58	3.22	3.10 ± 0.05	3.7	97.1
8	0.6	10.63	60	3.84	3.73 ± 0.04	2.9	261.2
13	0.6	11.22	61	4.13	3.97 ± 0.03	2.0	337.6
18	0.6	10.96	54	3.53	3.41 ± 0.03	3.6	389.1
22	0.6	10.46	53	3.32	3.16 ± 0.05	4.9	189.5

[a]The parameters of the PCEs were averaged over 10 PSCs. [b]The parallel resistance (R_p) and series resistance (R_s) for PSCs in the dark are obtained at around 0 and 1 V, respectively.

based on the P3HT:PCBM and P3HT:ICBA systems are 2.0 and 2.8 Ω cm^2, respectively, smaller than those of the PEDOT:PSS- and α-NiAc-modified PSCs. The decreased R_s is conducive to charge transport, thus leading to relatively high J_{sc}. Under illumination, the control devices based on P3HT:PCBM with PEDOT:PSS or α-NiAc as the buffer layer show different $J-V$ characteristics. V_{oc} dramatically decreases from 0.59 to 0.5 V when using α-NiAc instead of PEDOT:PSS as the anode buffer layer. The PCE obtained from the α-NiAc-buffered device (3.76%) is the same as that from the PEDOT:PSS-buffered device (3.77%), although it has a much higher J_{sc} of 11.36 mA cm^{-2}. From the UPS data, the WF of α-NiAc is only 4.24 eV, much lower than the HOMO level of P3HT (4.76 eV), which results in nonohmic contact between the P3HT and α-NiAc layers, leading to a relatively low V_{oc} for device B. After UVO treatment, the O-NiAc-buffered device C shows a high V_{oc} of 0.6 V, while maintaining a high J_{sc} of 11.22 mA cm^{-2}, leading to an increased maximum PCE of 4.13%. The WF of the nickel complex buffer layer can be increased to 4.93 eV after UVO treatment, higher than the HOMO level of P3HT. Therefore, the enhanced V_{oc} for device C can be ascribed to the ohmic contact formed between the O-NiAc buffer and photoactive layers. Although some previous literature reported that the appropriate UVO treatment could increase the WF of PEDOT:PSS and lead to enhancement in the device performance,[45,46] the devices with a UVO-treated PEDOT:PSS anode buffer layer show a deteriorated performance in our experiments (as shown in Figure S1 in the SI), which may be attributed to the breaking of polymer chains in the PEDOT:PSS film due to the UVO treatment. Similar results are obtained for P3HT:ICBA-based devices. P3HT:ICBA-based PSCs show higher V_{oc} than P3HT:PCBM-based PSCs because ICBA possesses a higher LUMO (0.17 eV) level than PCBM. The O-NiAc-buffered device F exhibits a higher V_{oc} of 0.88 V, compared to the α-NiAc-buffered device E, while maintaining a high J_{sc} of 10.36 mA cm^{-2} and a high FF of 72%, leading to an increased maximum PCE of 6.64%.

Figure 7 shows the $J-V$ curves of the PSCs with different O-NiAc thicknesses. The device parameters are listed in Table 2. R_p and FF increase with an increase of the O-NiAc buffer layer thickness, which could be attributed to the fact that the thicker buffer layer can efficiently suppress the leakage current caused by pinholes or other defects. However, excessive thickness of the O-NiAc buffer layer increases R_s of the PSCs, resulting in a decline in J_{sc}. All of the above factors lead to the determination that the optimal thickness of the O-NiAc buffer layer is around 15 nm.

4. CONCLUSIONS

In conclusion, efficient PSCs with enhanced V_{oc} are realized by UVO treatment of the NiAc anode buffer layer. The resultant dipole species, NiOOH, formed at the surface of the buffer layer during UVO treatment leads to an increase in the WF from 4.24 to 4.93 eV. Therefore, ohmic contact between the anode and photoactive layer can be formed, and the leakage current can be efficiently suppressed. For the PSCs based on the P3HT:PCBM system, V_{oc} increases from 0.50 to 0.60 V after the NiAc buffer layer undergoes UVO treatment. Similarly, in the P3HT:ICBA system, V_{oc} of the device with a UVO-treated NiAc buffer layer increases from 0.78 to 0.88 V, inducing an enhanced PCE of 6.64%. The results demonstrate that the UVO treatment is a simple but effective approach to improving V_{oc} in PSCs for high performance.

■ ASSOCIATED CONTENT

Supporting Information

$J-V$ curves and device parameters of the PSCs based on P3HT:PCBM and P3HT:ICBA using UVO-treated PEDOT:PSS as an anode buffer layer. This material is available free of charge via the Internet at http://pubs.acs.org.

■ AUTHOR INFORMATION

Corresponding Authors

*E-mail: tanzhanao@ncepu.edu.cn.
*E-mail: liyf@iccas.ac.cn.

Notes

The authors declare no competing financial interest.

■ ACKNOWLEDGMENTS

The work was supported by the NSFC (Grants 51173040, 91023039, and 51303052), the Ministry of Science and Technology of China (863 Project; Grant 2011AA050523), SRFDP (Grant 20130036110007), Program for New Century Excellent Talents in University (NCET-12-0848), Beijing Higher Education Young Elite Program (YETP0713), the 111 Project (B12034), and Fundamental Research Funds for the Central Universities, China (Grants 13ZD11, 2014ZD11, and 2014MS35).

■ REFERENCES

(1) Kim, J. Y.; Lee, K.; Coates, N. E.; Moses, D.; Nguyen, T. Q.; Dante, M.; Heeger, A. J. Efficient Tandem Polymer Solar Cells Fabricated by All-Solution Processing. *Science* **2007**, *317*, 222−225.
(2) Service, R. F. Outlook Brightens for Plastic Solar Cells. *Science* **2011**, *332*, 293−293.
(3) Tan, Z. A.; Zhang, W. Q.; Zhang, Z.; Qian, D. P.; Huang, Y.; Hou, J.; Li, Y. F. High-Performance Inverted Polymer Solar Cells with Solution-Processed Titanium Chelate as Electron-Collecting Layer on ITO Electrode. *Adv. Mater.* **2012**, *24*, 1476−1481.
(4) He, Z. C.; Zhong, C. M.; Su, S. J.; Xu, M.; Wu, H. B.; Cao, Y. Enhanced Power-Conversion Efficiency in Polymer Solar Cells Using an Inverted Device Structure. *Nat. Photonics* **2012**, *6*, 593−597.

(5) Yang, T. B.; Wang, M.; Duan, C. H.; Hu, X. W.; Huang, L.; Peng, J. B.; Huang, F.; Gong, X. Inverted Polymer Solar Cells with 8.4% Efficiency by Conjugated Polyelectrolyte. *Energy Environ. Sci.* **2012**, *5*, 8208−8214.
(6) You, J. B.; Dou, L. T.; Yoshimura, K.; Kato, T.; Ohya, K.; Moriarty, T.; Emery, K.; Chen, C.-C.; Gao, J.; Li, G.; Yang, Y. A Polymer Tandem Solar Cell with 10.6% Power Conversion Efficiency. *Nat. Commun.* **2013**, *4*, 1446.
(7) Ratcliff, E. L.; Meyer, J.; Steirer, K. X.; Garcia, A.; Berry, J. J.; Ginley, D. S.; Olson, D. C.; Kahn, A.; Armstrong, N. R. Evidence for near-Surface NiOOH Species in Solution-Processed NiO_x Selective Interlayer Materials: Impact on Energetics and the Performance of Polymer Bulk Heterojunction Photovoltaics. *Chem. Mater.* **2011**, *23*, 4988−5000.
(8) Steim, R.; Kogler, F. R.; Brabec, C. J. Interface Materials for Organic Solar Cells. *J. Mater. Chem. A* **2010**, *20*, 2499−2512.
(9) Hains, A. W.; Liu, J.; Martinson, A. B. F.; Irwin, M. D.; Marks, T. J. Anode Interfacial Tuning via Electron-Blocking/Hole-Transport Layers and Indium Tin Oxide Surface Treatment in Bulk-Heterojunction Organic Photovoltaic Cells. *Adv. Funct. Mater.* **2010**, *20*, 595−606.
(10) Potscavage, W. J.; Sharma, A.; Kippelen, B. Critical Interfaces in Organic Solar Cells and Their Influence on the Open-Circuit Voltage. *Acc. Chem. Res.* **2009**, *42*, 1758−1767.
(11) Friedel, B.; Keivanidis, P. E.; Brenner, T. J. K.; Abrusci, A.; McNeill, C. R.; Friend, R. H.; Greenham, N. C. Effects of Layer Thickness and Annealing of PEDOT:PSS Layers in Organic Photodetectors. *Macromolecules* **2009**, *42*, 6741−6747.
(12) Pingree, L. S. C.; MacLeod, B. A.; Ginger, D. S. The Changing Face of PEDOT:PSS Films: Substrate, Bias, and Processing Effects on Vertical Charge Transport. *J. Phys. Chem. C* **2008**, *112*, 7922−7927.
(13) Blom, P. W. M.; Mihailetchi, V. D.; Koster, L. J. A.; Markov, D. E. Device Physics of Polymer: Fullerene Bulk Heterojunction Solar Cells. *Adv. Mater.* **2007**, *19*, 1551−1566.
(14) Mandoc, M. M.; Koster, L. J. A.; Blom, P. W. M. Optimum Charge Carrier Mobility in Organic Solar Cells. *Appl. Phys. Lett.* **2007**, *90*, 133504.
(15) Tan, Z. A.; Qian, D. P.; Zhan, X. W.; Li, L. J.; Ding, Y. Q.; Xu, Q.; Wang, F. Z.; Li, Y. F. Efficient and Stable Polymer Solar Cells with Solution Processed Molybdenum Oxide Interfacial Layer. *J. Mater. Chem. A* **2013**, *1*, 657−664.
(16) Yang, T.; Wang, M.; Cao, Y.; Huang, F.; Huang, L.; Peng, J.; Gong, X.; Cheng, S. Z. D.; Cao, Y. Polymer Solar Cells with a Low-Temperature-Annealed Sol−Gel-Derived MoO_x Film as a Hole Extraction Layer. *Adv. Energy Mater.* **2012**, *2*, 523−527.
(17) Hammond, S. R.; Meyer, J.; Widjonarko, N. E.; Ndione, P. F.; Sigdel, A. K.; Garcia, A.; Miedaner, A.; Lloyd, M. T.; Kahn, A.; Ginley, D. S.; Berry, J. J.; Olson, D. C. Low-Temperature, Solution-Processed Molybdenum Oxide Hole-Collection Layer for Organic Photovoltaics. *J. Mater. Chem. A* **2012**, *22*, 3249.
(18) Girotto, C.; Voroshazi, E.; Cheyns, D.; Heremans, P.; Rand, B. P. Solution-Processed MoO_3 Thin Films as a Hole-Injection Layer for Organic Solar Cells. *ACS Appl. Mater. Interfaces* **2011**, *3*, 3244−3247.
(19) Wong, K. H.; Ananthanarayanan, K.; Luther, J.; Balaya, P. Origin of Hole Selectivity and the Role of Defects in Low-Temperature Solution-Processed Molybdenum Oxide Interfacial Layer for Organic Solar Cells. *J. Phys. Chem. C* **2012**, *116*, 16346−16351.
(20) Wong, K. H.; Ananthanarayanan, K.; Heinemann, M. D.; Luther, J.; Balaya, P. Enhanced Photocurrent and Stability of Organic Solar Cells Using Solution-Based NiO Interfacial Layer. *Sol. Energy* **2012**, *86*, 3190−3195.
(21) Steirer, K. X.; Ndione, P. F.; Widjonarko, N. E.; Lloyd, M. T.; Meyer, J.; Ratcliff, E. L.; Kahn, A.; Armstrong, N. R.; Curtis, C. J.; Ginley, D. S.; Berry, J. J.; Olson, D. C. Enhanced Efficiency in Plastic Solar Cells via Energy Matched Solution Processed NiO_x Interlayers. *Adv. Energy Mater.* **2011**, *1*, 813−820.
(22) Steirer, K. X.; Chesin, J. P.; Widjonarko, N. E.; Berry, J. J.; Miedaner, A.; Ginley, D. S.; Olson, D. C. Solution Deposited NiO Thin Films as Hole Transport Layers in Organic Photovoltaics. *Org. Electron.* **2010**, *11*, 1414−1418.
(23) Xu, Q.; Wang, F. Z.; Tan, Z. A.; Li, L. J.; Li, S. S.; Hou, X. L.; Sun, G.; Tu, X. H.; Hou, J. H.; Li, Y. F. High-Performance Polymer Solar Cells with Solution-Processed and Environmentally Friendly CuO_x Anode Buffer Layer. *ACS Appl. Mater. Interfaces* **2013**, *5*, 10658−10664.
(24) Tan, Z. A.; Li, L. J.; Wang, F. Z.; Xu, Q.; Li, S. S.; Sun, G.; Tu, X. H.; Hou, X. L.; Hou, J. H.; Li, Y. F. Solution-Processed Rhenium Oxide: A Versatile Anode Buffer Layer for High Performance Polymer Solar Cells with Enhanced Light Harvest. *Adv. Energy Mater.* **2014**, *4*, 1300884.
(25) Tan, Z. A.; Zhang, W. Q.; Cui, C. H.; Ding, Y. Q.; Qian, D. P.; Xu, Q.; Li, L. J.; Li, S. S.; Li, Y. F. Solution-Processed Vanadium Oxide as a Hole Collection Layer on an ITO Electrode for High-Performance Polymer Solar Cells. *Phys. Chem. Chem. Phys.* **2012**, *14*, 14589−14595.
(26) Zilberberg, K.; Trost, S.; Schmidt, H.; Riedl, T. Solution Processed Vanadium Pentoxide as Charge Extraction Layer for Organic Solar Cells. *Adv. Energy Mater.* **2011**, *1*, 377−381.
(27) Trost, S.; Zilberberg, K.; Behrendt, A.; Riedl, T. Room-Temperature Solution Processed SnO_x as an Electron Extraction Layer for Inverted Organic Solar Cells with Superior Thermal Stability. *J. Mater. Chem. A* **2012**, *22*, 16224−16229.
(28) Tan, Z. A.; Li, L. J.; Cui, C. H.; Ding, Y. Q.; Xu, Q.; Li, S. S.; Qian, D. P.; Li, Y. F. Solution-Processed Tungsten Oxide as an Effective Anode Buffer Layer for High-Performance Polymer Solar Cells. *J. Phys. Chem. C* **2012**, *116*, 18626−18632.
(29) Chen, Q.; Zhou, H.; Hong, Z.; Luo, S.; Duan, H. S.; Wang, H. H.; Liu, Y.; Li, G.; Yang, Y. Planar Heterojunction Perovskite Solar Cells via Vapor-Assisted Solution Process. *J. Am. Chem. Soc.* **2014**, *136*, 622−5.
(30) Zhang, W. Q.; Tan, Z. A.; Qian, D. P.; Xu, Q.; Li, L. J.; Li, S. S.; Wang, F. Z.; Zheng, H.; Li, Y. F. Using Water-Soluble Nickel Acetate as Hole Collection Layer for Stable Polymer Solar Cells. *J. Appl. Polym. Sci.* **2013**, *128*, 684−690.
(31) Tan, Z. A.; Zhang, W. Q.; Qian, D. P.; Cui, C. H.; Xu, Q.; Li, L. J.; Li, S. S.; Li, Y. F. Solution-Processed Nickel Acetate as Hole Collection Layer for Polymer Solar Cells. *Phys. Chem. Chem. Phys.* **2012**, *14*, 14217−14223.
(32) Scharber, M. C.; Mühlbacher, D.; Koppe, M.; Denk, P.; Waldauf, C.; Heeger, A. J.; Brabec, C. J. Design Rules for Donors in Bulk-Heterojunction Solar Cells—Towards 10% Energy-Conversion Efficiency. *Adv. Mater.* **2006**, *18*, 789.
(33) Snaith, H. J.; Greenham, N. C.; Friend, R. H. The Origin of Collected Charge and Open-Circuit Voltage in Blended Polyfluorene Photovoltaic Devices. *Adv. Mater.* **2004**, *16*, 1640−1645.
(34) Yuan, Y.; Reece, T. J.; Sharma, P.; Poddar, S.; Ducharme, S.; Gruverman, A.; Yang, Y.; Huang, J. Efficiency Enhancement in Organic Solar Cells with Ferroelectric Polymers. *Nat. Mater.* **2011**, *10*, 296−302.
(35) Maurano, A.; Hamilton, R.; Shuttle, C. G.; Ballantyne, A. M.; Nelson, J.; O'Regan, B.; Zhang, W.; McCulloch, I.; Azimi, H.; Morana, M.; Brabec, C. J.; Durrant, J. R. Recombination Dynamics as a Key Determinant of Open Circuit Voltage in Organic Bulk Heterojunction Solar Cells: a Comparison of Four Different Donor Polymers. *Adv. Mater.* **2010**, *22*, 4987−4992.
(36) Lee, T.-W.; Chung, Y. Control of the Surface Composition of a Conducting-Polymer Complex Film to Tune the Work Function. *Adv. Funct. Mater.* **2008**, *18*, 2246−2252.
(37) Helander, M. G.; Wang, Z. B.; Greiner, M. T.; Liu, Z. W.; Lian, K.; Lu, Z. H. The Effect of UV Ozone Treatment on Poly(3,4-ethylenedioxythiophene):poly(styrenesulfonate). *Appl. Phys. Lett.* **2009**, *95*, 173302.
(38) Lee, H. K.; Kim, J.-K.; Park, O. O. Effects of UV Light-Irradiated Buffer Layer on the Performance of Polymer Solar Cells. *Org. Electron.* **2009**, *10*, 1641−1644.
(39) Adhikary, P.; Venkatesan, S.; Adhikari, N.; Maharjan, P. P.; Adebanjo, O.; Chen, J.; Qiao, Q. Enhanced Charge Transport and

Photovoltaic Performance of PBDTTT-C-T/$PC_{70}BM$ Solar Cells via UV-ozone Treatment. *Nanoscale* **2013**, *5*, 10007−10013.
(40) Zhai, Z.; Huang, X.; Xu, M.; Yuan, J.; Peng, J.; Ma, W. Greatly Reduced Processing Temperature for a Solution-Processed NiO_x Buffer Layer in Polymer Solar Cells. *Adv. Energy Mater.* **2013**, *3*, 1614−1622.
(41) Hou, J. H.; Tan, Z. A.; Yan, Y.; He, Y. J.; Yang, C. H.; Li, Y. F. Synthesis and Photovoltaic Properties of Two-Dimensional Conjugated Polythiophenes with Bi(thienylenevinylene) Side Chains. *J. Am. Chem. Soc.* **2006**, *128*, 4911−4916.
(42) He, Y. J.; Zhao, G. J.; Peng, B.; Li, Y. F. High-Yield Synthesis and Electrochemical and Photovoltaic Properties of Indene-C_{70} Bisadduct. *Adv. Funct. Mater.* **2010**, *20*, 3383−3389.
(43) He, Y. J.; Chen, H. Y.; Hou, J. H.; Li, Y. F. Indene-C_{60} Bisadduct: A New Acceptor for High-Performance Polymer Solar Cells. *J. Am. Chem. Soc.* **2010**, *132*, 1377−1382.
(44) Steirer, K. X.; Chesin, J. P.; Widjonarko, N. E.; Berry, J. J.; Miedaner, A.; Ginley, D. S.; Olson, D. C. Solution Deposited NiO Thin Films as Hole Transport Layers in Organic Photovoltaics. *Org. Electron.* **2010**, *11*, 1414−1418.
(45) Su, Z.; Wang, L.; Li, Y.; Zhao, H.; Chu, B.; Li, W. Ultraviolet-Ozone-Treated PEDOT:PSS as Anode Buffer Layer for Organic Solar Cells. *Nanoscale Res. Lett.* **2012**, *7*, 465.
(46) Helander, M. G.; Wang, Z. B.; Greiner, M. T.; Liu, Z. W.; Lian, K.; Lu, Z. H. The Effect of UV Ozone Treatment on Poly(3,4-ethylenedioxythiophene):poly(styrenesulfonate). *Appl. Phys. Lett.* **2009**, *95*, 173302.